Indian Journal of Marine Sciences
Vol. 37(1), March 2008, pp. 77-85

Simulation of Antarctic sea ice area with artificial neural network

K. C. Tripathi & I. M. L. Das*
K.Banerjee Center of Atmospheric & Ocean Studies, University of Allahabad, Allahabad – 211002, U. P., India
*[E-mail: drimldas@yahoo.com]

The artificial neural network (ANN) has been used for simulation of Antarctic sea ice area anomalies. Various dominant cycles present in the data have been identified using the Fourier analysis. It has been found that the data of the Antarctic sea ice area has two dominant cycles: annual and half yearly. The effect of the presence and / or absence of these dominant cycles on the simulation results have been carried out. ANN can simulate the broad trend of the sea ice area anomalies when all the cycles are present. However, the prediction skill of model for intraseasonal variability degrades as we remove the trends. Further, the forecast have been verified on the basis of various attributes of the forecast.

[**Keywords:** Artificial neural network, Antarctic sea ice, Fourier analysis, activation function, sea ice, simulation, forecast, error back propagation]

1. Introduction

The salt / freshwater and heat exchanges between sea ice and ocean are crucial in the Southern Ocean for the deep water production, its properties and export. The large amount of brine released during ice formation on the Antarctic continental shelf leads to very high salinities there. The resulting dense shelf waters are then transported toward great depths after some mixing with ambient waters, finally forming the Antarctic Bottom Water body[1,2]. Besides, the net ice melting associated with ice convergence in some areas, such as the southwestern Pacific, stabilizes the water column and forbids deep mixing in these regions. Furthermore, the contact with the ice imposes that the polar surface waters must be maintained very close to their freezing point temperature. This process takes an important part in increasing the density of the Antarctic Bottom Water.

Due to the seasonal variation in insolation, seawater freezes over the surface of polar ocean producing a thin but discontinuous blanket of sea ice over, on which snow can accumulate. Sea ice covers roughly 7% of world's ocean (~23.5 millions km^2) and accounts for about two third of Earth's ice cover[3, 4]. Its global extent oscillates between ~30 × 10^6 km^2 (during the austral winter) and ~ 20 × 10^6 km^2 (during the austral summer)[5]. Contrary to several hundreds - meter thick continental ice sheet, the sea ice is very thin whose thickness and aerial extent responds quickly to the change in surface heat balance, thus modulating the interaction between the atmosphere and the ocean on timescales ranging from months to years.

Polar geophysical processes play an important role in maintaining the thermodynamics balance of Earth's climate system. Sea ice is a key component of this system and accurate information about sea ice dynamics, melting events and numerous feedback processes are needed for understanding climate variability and trends[6-11]. Sea ice modulates the short wave albedo, heat, moisture, and momentum between the atmosphere and ocean which in turn modulates the climate[12-15]. Sea ice is characterized by significant interannual variability[16-21]. Recently, changes and trends in polar sea ice cover have been intensively investigated after the availability of microwave data from satellites[22-33]. More research is needed tounderstand how interactions among atmospheric circulation, sea ice motion, and sea ice melt dynamics in the polar region could significantly affect the behavior of ice-albedo feedbacks or ocean-atmosphere heat fluxes in global climate models[34, 35]. Further, polar sea ice extent is closely related to the dire phenomenon of global warming.

Recently, due to the increasing realization of the importance of sea ice in global weather and climate system, various aspects of sea ice have been studied using artificial neural networks[36-43]. In the present paper we investigate the possibility of predicting the Antarctic sea ice variability using artificial neural

*Corresponding author
Phone: +91-532-2460974
Fax: 91-532-2460974

networks. It has been found that the Antarctic sea ice anomalies can be successfully predicted with a reasonably good accuracy.

2. Artificial Neural Networks

Artificial neural networks (ANNs) are modeled on the operating behavior of the brain and are especially useful for classification and function approximation / mapping problems, to which mathematical descriptions cannot be specified easily. Contrary to linear modeling techniques, ANNs are inherently nonlinear and learn by examples. The ANNs are better suited for prediction because noise patterns and chaotic components are better tolerated by them than by other statistical methods[44]. The prediction and classification capability of the ANNs has been found to be far more superior to the other traditional methods[45, 46]. Studies have also shown that not only ANN performs better than the traditional multivariate regression model but that it can predict the future in cases where the regression model fails to make any forecast at all[47].

ANN is now widely used in oceanography and meteorology for the prediction and modeling of various atmospheric and oceanic phenomena. Some of the recent examples include: prediction of tsunami travel time in the Indian ocean[48], predictability of sea surface temperature[47], nonlinear canonical correlation analysis for the study of relationship between the tropical pacific sea level pressure and the sea surface temperature[49] and Nonlinear principal component analysis[50]. ANNs are gradually finding more and more applications in the study of Arctic and Antarctic sea ice such as Retrieval of Antarctic sea ice pressure ridge[51] and sea ice classification[52].

In the present study we use a multi-layer feed forward artificial neural network. A typical multi-layer feed forward ANN consists of inter-connected set of processing units called neurons. These neurons are organized in three distinct layers: Input layer, hidden layer and output layer as shown in Figure 1. These layers are connected via neuronal links: two neurons i and j of the two consecutive layers have synaptic connections associated with a synaptic weight W_{ij}. Each neuron j performs two specific operations:

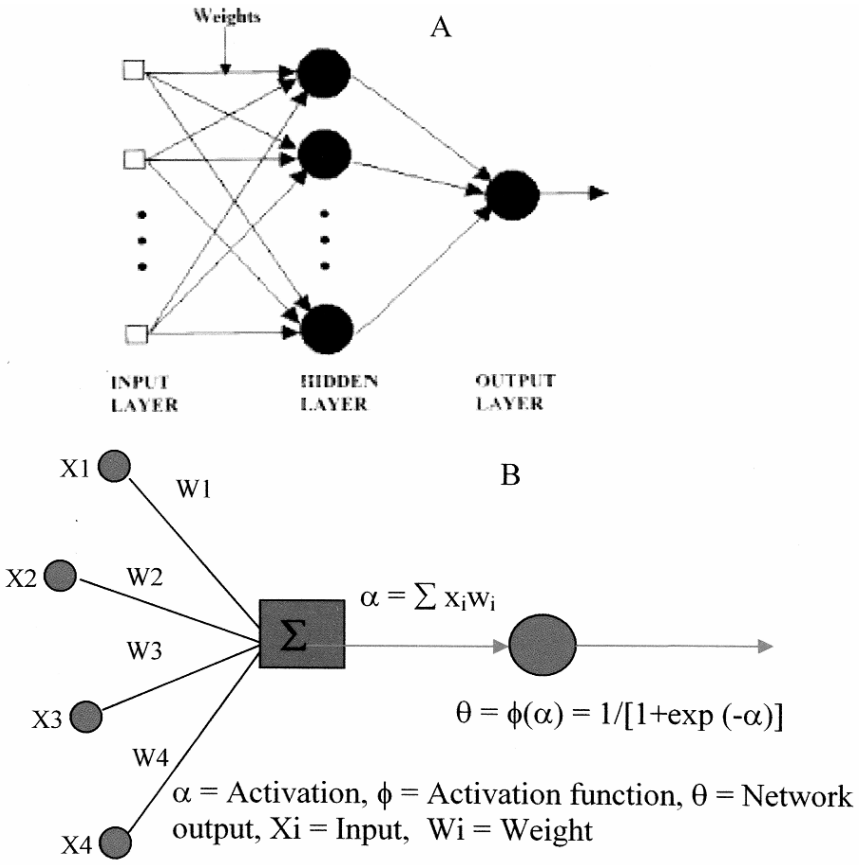

Fig. 1—(A): A typical example of neural network (B): Working of a neuron with the sigmoid activation function.

(i) It makes a weighted sum of its inputs from the previous layer I_i. This is called the activity signal a_j of the neuron given by

$$a_j = \sum_i (W_{ij} I_i + B_j)$$

where B_j is bias.

(ii) Then, it transfers this activity signal to its output through a so-called 'transfer function', say σ. The output O_j of the neuron j in the hidden layer is given by

$$O_j = \sigma(\sum_i W_{ij} I_i)$$

The 'transfer function' σ can have several forms such as nonlinear sigmoid function, simple linear activation, threshold activation and hyperbolic tangent activation. However, we have used the most prevalent and commonly used sigmoid function[44]

$$F(x) = 1/[1 + \exp(-x)]$$

as the activation function. Generally, neurons of the output layer use identity function as transfer function. We have used the identity function[50]

$$f(\alpha) = \alpha$$

as the activation function for the neurons in the output layer.

It is critical to identify the appropriate training interval. If the training interval is too short, the ANN cannot learn all patterns and prediction accuracy is low. If the training interval is too long, neural networks begin to fit the noise present in the training data leading to overtraining[44]. When such a over trained network is presented with data that it has not yet seen (i.e., data with the same relationship as the training data, but with new and different noise), its performance is lower than if it had only learned the actual relationship during training. We identify the proper training interval by comparing the performance of the ANN on data that it has not yet seen (i.e., test data) after different training intervals. Network performance should increase as the training interval increases until the ANN overfits the training data, at which point performance will decrease. Because the overtrained ANN learns the noise of a particular training dataset, we assess the performance using different training and testing datasets. We create the training and testing datasets by randomly separating the data.

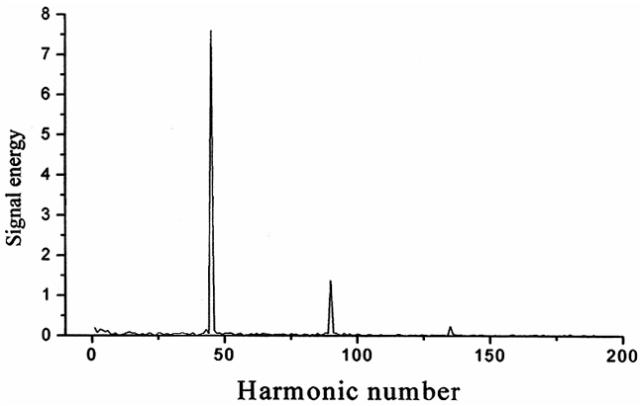

Fig. 2—Power spectra of the sea ice data.

3. Methodology

3.1 Data

There have been very few systematic observations of Antarctic sea ice parameters and the available records are short. As such the spatial and temporal (seasonal) variability of Antarctic sea ice is not well understood[53]. The observed data of Antarctic sea ice area (daily)[54] for the 45-year period from January 1948 to December 1992 has been used for the present analysis. This data has been derived from passive microwave measurements by applying the Bootstrap algorithm[55].

3.2 Preprocessing

The first step in the preprocessing is to identify the climatologic component. This has been done by the spectral analysis using the Fourier transformations[56]. The power spectrum of sea ice area is shown in Figure 2 from which two dominant cycles have been identified in the time series for Antarctic sea ice area. These are the 45th harmonic (corresponding to a period of 365 days i.e. one year) and the 90th harmonic (corresponding to a period of 182.5 days i.e. 6 months). The simulation experiment has been conducted in three steps: (i) Simulation without removing the dominant cycles to predict the broad climatology of sea ice area anomaly, (ii) Simulation after removing the first dominant component (45th harmonic) and (iii) Simulation after removing the first two dominant components (45th and 90th harmonics). Simulation after removing the dominant components was performed to evaluate the performance of the model in predicting the intra-seasonal variability of sea ice area anomaly.

The area anomaly was calculated and correlation

analysis done to determine the predictors. The correlation with lag from 1 day to 365 days has been evaluated. It has been found that the series with 1-year lag has the best correlation with the current series. Hence the 1-year lag series has been used as the predictor.

The predictor and the predictand series has been normalized using the following scheme

$$X_n = [(X - X_{\min})/(X_{\max} - X_{\min}) * 0.6 + 0.2 \qquad (1)$$

where X is the sea ice area anomaly, $X_{\max}$ is the maximum anomaly for the month, $X_{\min}$ is the minimum anomaly for the month and X_n is the normalized value of the anomaly. The factors of 0.6 and 0.2 are included so that the normalized values are not 0.0 or 1.0. As X_n approaches these extreme values, the derivative of the sigmoid function becomes 0 and no learning occurs[57].

3.3 Partitioning of data

The normalized data is partitioned into three sets namely the training, validation and the test set. The full time series for area anomaly for 45 years consists of 16425 points. Since 1-year lag series has been used as the predictor, the effective number of input-output pairs reduces to 16060. Of these 16060 ordered pairs, 13140 pairs (approximately 80%) is used to "train" the network. These pairs form the "training set". The ANN determines the optimum relationship between these input-output pairs by optimizing the free parameters, which in this case is the value of the weight matrix. Minimizing a cost function, which in this case is the mean square error between the model output and the observations in the training set, does the optimization of the free parameters. The remaining 20% of the input-output pairs are used for assessing the mapping obtained by the ANN on the unseen data. The performance evaluation on the unseen data has been done in two phases: (i) the online phase called the cross-validation and (ii) the offline phase called the testing. For the cross-validation, 63% (of the pairs that were not used in training) data, i.e. 1825 patterns, have been used. For the testing, or hindcast, 37% (of the pairs that were not used in training) data, i.e. 1095 patterns, have been used.

3.4 Architecture of the ANN

The architecture of the ANN used in the present study is shown in Figure 1. The number of neurons in the input, output and hidden layers are 1, 5 and 1 respectively. It has been proved that one hidden layer is sufficient to model arbitrary complexity in the data[58]. Each neuron in the hidden layer of an ANN is dedicated to learn some non-linearity in the data. So the number of neuron in the hidden layer must not be less than the required number as this will deprive the network of the resources to learn the non-linearity in the data. Increasing the number of hidden layer neurons beyond the required number will complicate the architecture, by increasing the number of free parameters. This will increase the amount the data required to train the network. But training data is fixed. So the overall effect of further increasing the number of hidden layer neurons is that the free parameters are increased without increasing the amount of data required to optimize those parameters thus rendering the network to be overfitted[59], a common problem encountered in all statistical models.

4. Results and Discussion

The performance of the model without removing any cycles (1st case) for the training and the test sets are shown in Figure 3. The correlation coefficient for both training and test cases are found to be 0.96. The root mean square error (RMSE) and standard deviation (SD) for observed data are 1.82 and 5.52 for training and 1.70 and 5.18 for test cases respectively. As the RMSE is significantly smaller than the SD of the observed data, we infer that the model prediction is better than the mean prediction. Thus, the prediction skill of the model for simulating the broad features of sea ice area anomaly is reasonably good with a very high degree of accuracy.

The performance of the model after removing the first dominant cycle (2nd case) for the training and the test cases are shown in Figure 4. The correlation coefficients are found to be 0.89 and 0.94 for training and test cases respectively. The RMSE and SD for observed data are 0.51 and 1.1 for training and 0.36 and 0.99 for test cases respectively. Similarly, Figure 5 shows the performance of the model after removing the two most dominant cycles (3rd case) for the training and the test cases. In this case, the RMSE and SD for observed data are 0.44 and 0.49 for training and 0.36 and 0.42 for test cases respectively. The correlation coefficients are found to be 0.43 and 0.66 for training and test cases respectively. Thus, after removing all the trends and analyzing the results, we get a significant correlation coefficient although we

are predicting one year in advance. The small value of RMSE compared to the SD of the observed data indicates that the prediction is better than the mean prediction. However, the predicted area anomaly almost looks like the mean value as RMSE and the standard deviation of the observed data are very close to each other. Thus, it can be seen that the prediction skill of model for intraseasonal variability degrades as we remove the trends.

The quality of every forecast has to be determined by the so-called forecast verification process. The forecast verification process involves comparison of matched pairs of forecasts and observations. There are several reasons (administrative, economic and scientific) to objectively evaluate the forecast quality and the most important amongst them is to assess the strengths and weaknesses of the forecast for further improvement.

For evaluating the quality of forecast based on binary or dichotomous (yes/no) forecasts, the test data has been classified in two classes; normal event and rare event. A normal event is one when the observed sea ice area anomaly is under the standard deviation of the observed data. A rare event is defined as the case when the observed sea ice area anomaly exceeds the standard deviation of the observed data. In the

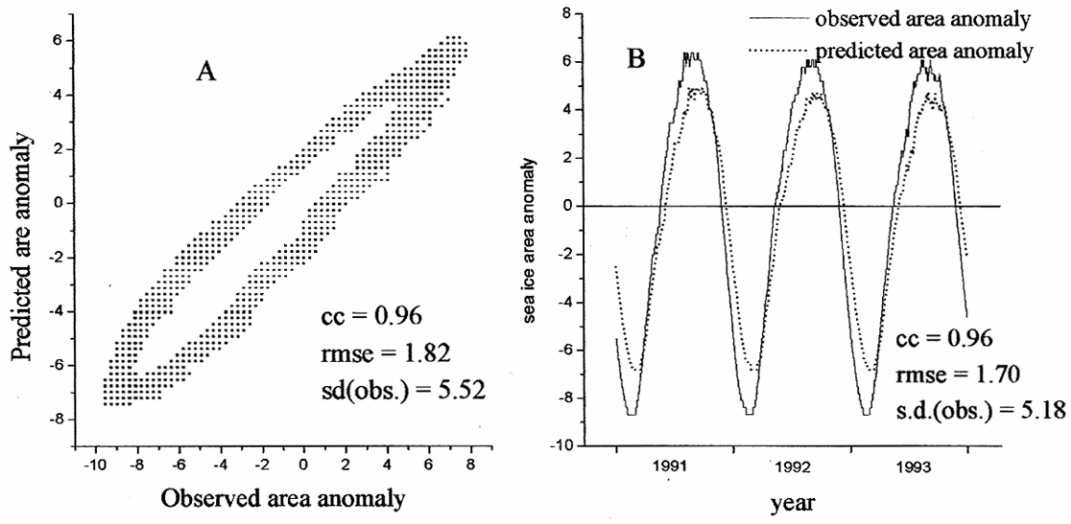

Fig. 3—Comparison of observed and simulated anomalies without removing climatology and other cycles (A): training case, (B): test case

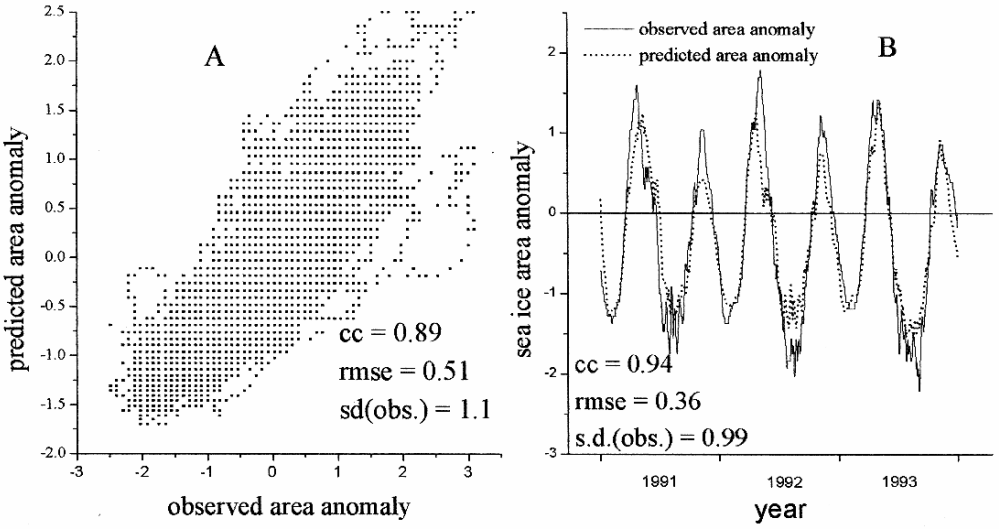

Fig. 4—Comparison of observed and simulated anomalies after removing climatology (annual cycle)— (A): training case, (B): test case

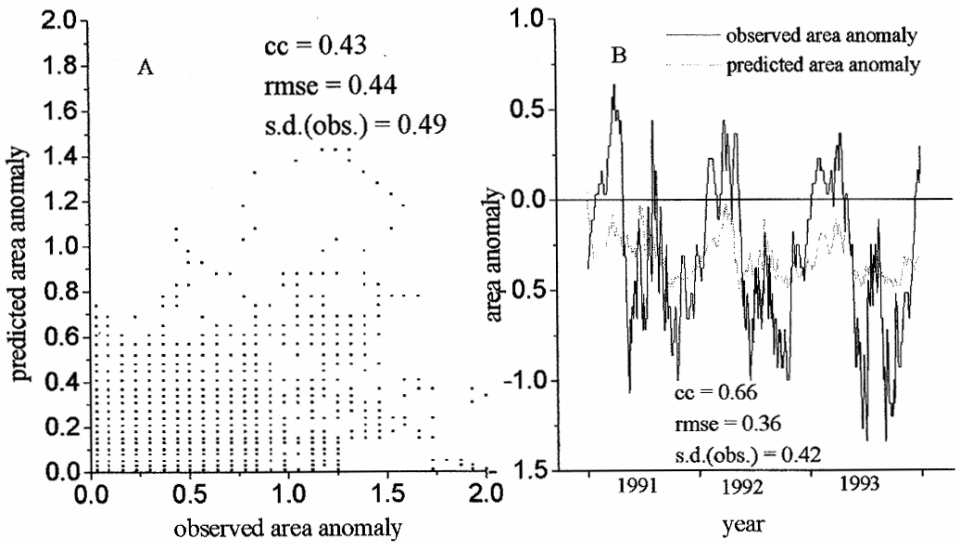

Fig. 5—Comparison of observed and simulated anomalies after removing the annual and six-monthly cycles— (A): training case, (B): test case

Table 1—Contingency tables for dichotomous forecasts

		Yes	No	Total
(A) All cycles present (1st case)				
Forecast	Yes	206	12	218
	No	315	562	877
	Total	521	574	1095
(B) Annual cycle removed (2nd case)				
Forecast	Yes	359	32	391
	No	182	522	704
	Total	541	554	1095
(C) Annual and six monthly cycles removed (3rd case)				
Forecast	Yes	250	61	311
	No	258	526	784
	Total	508	587	1095

present study, an “event” means a “rare event”. A dichotomous forecast says categorically whether or not the event will happen. The contingency table is a useful way to see what types of errors are being made. A perfect forecast system would produce only hits and correct negatives, and no misses or false alarms. A contingency table shows the frequency of “yes” and “no” forecasts and occurrences (Table 1).

Forecast skill refers to the relative accuracy of a set of forecasts with respect to some set of standard forecasts. One of the most common choices for the reference forecast is the climatological average of the predictand. Table 2 shows the various skill scores for the dichotomous forecasts for test cases. It may be seen that accuracy is 70% or more. This means that overall 70% of the forecasts are correct for the 1st and 3rd cases of the simulation and 80% of the forecasts are correct for the 2nd case of the simulation.

The bias term shows the fraction of the forecast frequency of the yes events and the observed frequency of the yes events. Ideally this fraction should be 1. In the worst case the ratio can be 0 (if there is no “yes” in the forecast set or infinity (if there is no “yes” in the observed case). If the bias term is greater than 1 then there is overforecast and if less than 1 then there is underforecast. In our case, there is underforecast in all the three cases.

The “probability of detection (POD)” indicates the fraction of the observed “yes” events that were correctly forecast. Ideally its value should be 1 and in the poorest case (when there are no “hits”) the value is 0. The probability of detection is best in the second case when the annual cycle is removed. The probability of detection should be used in conjunction with the false alarm ratio. The false alarm ratio is a measure of the fraction of the predicted “yes” events that actually did not occur (false alarm). The ideal value should be 0 and the worst case value is 1. In the present model we see that the false alarm ratio is very close to zero: 0.19 being the worst case and 0.06 being the best case.

Probability of false detection (POFD) is another attribute that tells us what fraction of the observed "no" events were incorrectly forecast as "yes". Ideally

Table 2—Forecast verification scores

	Acc.	Bias	POD	FAR	POFD	TS	ETS	HSS	OR
All cycles present (1st case)	0.70	0.42	0.39	0.06	0.02	0.39	0.24	0.38	31.32
Annual cycle removed (2nd case)	0.80	0.72	0.66	0.08	0.06	0.63	0.44	0.61	30.41
Annual and six monthly cycles removed (3rd case)	0.71	0.61	0.49	0.19	0.10	0.44	0.25	0.39	8.65

Acc. = Accuracy of forecast, Bias = Bias of forecast, POD = Probability Of Detection, FAR = False Alarm Ratio, POFD = Probability of False Detection, TS = Threat Score ETS = Equitable Threat Score, HSS = Heidke Skill Score, OR = Odds Ratio.

this should be zero. It is sensitive to the climatological frequency of the event. Again, we see that the POFD is very close to zero for all the cases. When observed in conjunction with the probability of detection, we see that the POD is much greater than POFD.

Threat score (TS) measures the degree of correspondence between the forecast "yes" events and the observed "yes" events. Perfect score is 1 and worst score is 0 that indicates no correspondence at all. In our study the TS is 0.63 (best case) when the first dominant (annual) cycle (2nd case) is removed and the worst case value is 0.39 when all the cycles are present (1st case). Threat score is normally used in conjunction with Equitable Threat Score (ETS). The allowed range of ETS is from -1/3 to 1 with 0 indicating no skill and 1 giving a perfect score. ETS Measures the fraction of observed and/or forecast events that were correctly predicted after adjusted for hits associated with random chance. It measures the same quantity but accounts for the "by chance" events. It is always less than the TS. The best case in our study is the case when the annual cycle was removed. We see that slightly less than half on the rare events were correctly forecast, taking into account the forecast that happened "by chance".

The Heidke Skill Score (HSS) measures the fraction of correct forecasts after eliminating those forecasts, which would be correct due purely to random chance. The range of HSS is from minus infinity to 1 with 0 indicating no skill and 1 giving a perfect score. In the present study, 2nd case gives better value for HSS as compared to the other cases.

Odds Ratio (OR) informs about the odds of a "yes" forecast being correct relative to the odds of the "yes" forecast being incorrect. In other words, it measures the ratio of the odds of making a hit to the odds of making a false alarm. It can have values between 0 to infinity: 1 indicating no skill and infinity for perfect score. In the present study, we see that OR is 31.32 for the 1st case. This means that the odds of a "yes" prediction being correct are over 31 times greater than the odds of a "yes" prediction being incorrect. The OR for the 2nd and 3rd cases is 30.41 and 8.65 respectively.

We have investigated the simulation of Antarctic sea ice using ANN on the basis of commonly used statistical parameters such as correlation coefficient, root mean square error and standard deviation. But these parameters are not sufficient to assess the quality of forecast. Therefore, various other attributes of the forecast[54] were also determined. On the basis of the analysis of these parameters and attributes we conclude that ANN is capable of simulating the Antarctic sea ice extent to a fairly good accuracy.

Acknowledgement

Authors are thankful to the National Centre for Antarctic and Ocean Research, Vasco da Gama, Goa, India and Ministry of Earth Sciences, Government of India for financial assistance.

References

1 Orisi, A.H., Johnson, G.C. & Bullister, J.L, Circulation, mixing and production of Antarctic bottom water, *Prog. Oceanogr*., 43(1999), 55-109.

2 Doney, S.C., & Hecht, W., Antarctic bottom water formation and deep-water chloroflurocarbon distributions in a global ocean climate model, *J.Phys. Oceanogr*., 32(2002), 1642-1666.

3 Barry, R. G., Aspects of the meteorology of the seasonal ice zone, in: *The geophysics of sea ice, NATO, ASI Series*, edited by N. Untersteiner, (Plenum Press, New York) 1986, pp. 993-1020.

4 Maykut, G. A. & Untersteiner, N., Some results from a time-dependent, hermodynamic model of sea ice, *J. Geophys. Res.*, 76 (1971) 1550-1575.

5 Gloersen, P., Campbell, W. J., Cavalieri, D. J., Comiso, J. C., Parkinson, C. L. & Zwally, H. J., *Arctic and Antarctic sea ice, 1978-1987: Satellite passive-microwave observations and analysis*, NASA SP-511 (Washington D. C, USA) 1992, pp. 290.

6 Manabe, S., Spelman, M. J. & Stouffer, R. J., Transient responses of a coupled ocean atmosphere model to gradual

changes in atmospheric CO2, *J. Climate*, 5 (1992) 105–126.
7 Barry, R. G., Serreze, M. C., Maslanik, J. A. & Preller, R. H.,The Arctic sea ice-climate system: observations and modeling, *Rev. Geophys*., 31 (1993) 397–422.
8 Thompson, D. W. J., & Wallace, J. W., The Arctic Oscillation signature in the wintertime geopotential height and temperature fields. *Geophys. Res. Lett.*, 25 (1998) 1297–1300.
9 Holland, D. M., An impact of subgrid-scale ice-ocean dynamics on sea-ice cover, *J. Climate*, 14 (2001) 1585–1601.
10 Parkinson C. L., Rind, D., Healy, G. J., & Martinson, D. G., The impact of sea ice concentration accuracies on climate model simulations with the GISS GCM, *J. Climate*, 14 (2001), 2606–2623.
11 Kukla, G., Central Arctic: Battleground of natural and man-made climate forcing, *Eos, AGU*, 85 (2004) 200-202.
12 Agnew, I., Simultaneous winter sea-ice and atmospheric circulation anomaly patterns, *Atmos. Ocean*, 31(1993) 259-280.
13 Chapman, W. L., & Walsh, J. E., Recent variations of sea ice and air temperature in high latitudes, *Bull. Amer. Meteor. Soc.*, 74 (1993) 33–47.
14 Deser, C., & Blackmon, M. L., Surface climate variation over the North Atlantic Ocean during winter: 1900–1989, *J. Climate*, 6 (1993) 1743–1753.
15 Deser C., Alexander, M. A. & Timlin, M. S., On the persistence of sea surface temperature anomalies in midlatitudes. *J. Climate* , 16 (2002) 57-72.
16 Walsh, J. E., & Johnson, C. M., An analysis of arctic sea ice fluctuations, 1953–1977, *J. Phys. Oceanogr.*, 9 (1979) 580-591.
17 Hibler, W. D., & Becky, R., Numerical simulation of northern hemisphere sea ice variability, 1951–1980, *J. Geophys. Res.*, 90 (1985) 4847–4865.
18 Fang, Z., & Wallace J. M., Arctic sea ice variability on a timescale of weeks: its relation to atmospheric forcing, *J. Climate*, 7(1994) 1897–1913.
19 Belchansky, G. I., Douglas, D. C. & Mordvintsev, I. N., Assessing trends in Arctic Sea Ice distribution using the «KOSMOS-OKEAN» satellite series, Polar Record, *Scott. Polar Research Inst.*, 31 (1995) 129-134.
20 Mysak L., Ingram, A., R. G., Wang, J. & Van Der Baaren A., The anomalous sea-ice extent in Hudson Bay, Baffin Bay and the Labrador Sea during three simultaneous ENSO and NAO episodes, *Atmos. Ocean*, 34 (1996) 313–343.
21 Deser, C., Walsh, J. E. & Timlin, M. S., Arctic sea ice variability in the context of recent atmospheric circulation trends, *J. Climate*, 13 (2000) 617–633.
22 Cavalieri, D. J., Burns, B. A. & Onstott, R. G., Investigation of the effects of summer melt on the calculation of sea ice concentration using active and passive microwave data, *J. Geophys. Res*., 95 (1990) 5339–5369.
23 Maslanik, J. A., Serreze, M. C. & Barry, R.G., Recent decreases in Arctic summer ice cover and linkages to atmospheric circulation anomalies, *Geophys. Res. Lett*., 23 (1996) 1677–1680.
24 Parkinson C. L., Cavalieri, D. J., Gloersen, P., Zwally, H.J. & Comiso, J. C., Arctic sea ice extents, areas, and trends, 1978–1996, *J. Geophys. Res.*, 104 (1999) 20837–20256.
25 Vinnikov K. Y., Robock, A., Stouffer, R. J., Walsh, J. E., Parkinson, C. L., Cavalieri, D. J., Mitchell, J. F. B., Garrett, D., & Zakharov, V. F., Global warming and northern hemisphere sea ice extent, *Science*, 286 (1999), 1934–1937.
26 Vinnikov, K. Y., Robock, A., Cavalieri, D. J., & Parkinson, C. L., Analysis of seasonal cycles in climatic trends with application to satellite observations of sea ice extent, *Geophys. Res. Lett. 29* (2002) 1310, doi:10.1029 / 2001GL014481.
27 Cavalieri, D. J., Parkinson, C. L., Gloersen, P., Comiso, J. C. & Zwally, H. J, Deriving long-term time series of sea ice cover from satellite passive-microwave multisensor data sets. *J. Geophys. Res*., 104 (1999) 803–15,814.
28 Johannessen, O. M., Shalina, E.S., & Miles, M.W., Satellite evidence for an Arctic sea ice cover in transformation, *Science*, *286* (1999), 1937–1939.
29 Parkinson C. L., & Cavalieri, D.J., A 21 year record of Arctic sea-ice extents and their regional, seasonal and monthly variability and trends, *Ann. Glaciol*., 34 (2002), 441–446.
30 Comiso, J. C., Satellite-observed variability and trend in sea-ice extent, surface temperature, albedo and clouds in the Arctic, *Ann. Glaciol*., 33 (2001) 457–473.
31 Comiso, J. C., Correlation and trend studies of the sea-ice cover and surface temperatures in the Arctic, *Ann. Glaciol*., 34 (2002) 420–428.
32 Comiso, J. C., A rapidly declining perennial sea ice cover in the Arctic, *Geophys. Res. Lett*., 29 (2002) 1956, doi:10.1029/2002GL015650.
33 Comiso, J. C.,Yang, J., Honjo, S. & Krishfield, R. A., Detection of change in the Arctic using satellite and in situ data, *J. Geophys. Res*., 108 (2003), doi:10.1029 /2002JC001347.
34 Belchansky, G. I., Douglas, D. C., Mordvitsev, I.N. & Platonov, N.G., Estimating the time of melt onset and freeze onset over Arctic sea-ice area using active and passive microwave data, *Remote Sens. Environ.*, 92 (2004) 21-39.
35 Belchansky, G. I., Douglas, D. C. & Platonov, N. G., Duration of the Arctic sea ice melt season: regional and interannual variability, 1979–2001, *J. Climate*, 17 (2004) 67-80.
36 Tovinkere V. R., Penaloza, M., Logar, A., Lee, J., Weger, R. C., Berendes, T. A. & Welch, R. M., An intercomparison of artificial intelligence aproaches for polar scene identification, *J. Geophys. Res.*, 98 (1993) 5001–5016.
37 Hara Y., R.G. Atkins, R.T. Shin, J.A. Kong, S.H. Yueh, & R. Kwok, Application of neural networks for sea ice classification in polarimetric SAR images, *IEEE Trans. Geosci. Rem. Sens*, 33 (1995), 740-748.
38 Belchansky, G. I., & Douglas, D. C., Classification methods for monitoring Arctic sea-ice using OKEAN passive/active two-channel microwave data, *J. Remote Sens. Environ.*, 73 (2000) 307–322.
39 Turner, J., Connolley, W., Cresswell, D. & Harangozo, S., The simulation of Antarctic sea ice in the Hadley Centre Climate Model (HadCM3), *Ann. Glaciol*, 33 (2001) 587-91.
40 El-Rabbany, A., Auda a1,G. & Abdelazim, S., Predicting sea ice conditions using neural networks, *J. Navigation*, 55 (2002) 137-143.
41 Belchansky G.I., Douglas D.C., Alpatsky I.V., & Platonov N.G., Spatial and temporal multiyear sea ice distributions in the Arctic: A neural network analysis of SSM/I data, 1988–2001. *J. Geophys. Res*., 109 (2004) doi:10.1029 / 2004JC002388.

42 Belchansky G.I., Douglas D.C., Eremeev V.A., & Platonov N.G., Variations in the Arctic's multiyear sea ice cover: A neural network analysis of SMMR-SSM/I data, 1979–2004, *Geophys. Res. Lett*., 32(2005) L09605, doi:10.1029-/2005GL022395.

43 Xavier, N., Nicolas, M. & Marc, A., Enhanced neural-network based sea / ice discrimination using ERS scatterometer data, in *Remote sensing of the ocean, sea ice, and large water regions,* edited by Bostater Charles R., Jr., Santoleri Rosalia, Proc. SPIE, 5977) 2005, pp. 55-64.

44 Masters, T., *Practical neural network recipes in C++*, (Academic Press, USA) 1993, pp. 10-300.

45 Weigend A.S., Gershenfeld N.A., *Time series prediction: Forecasting the future and understanding the past* (Proceedings of Santa Fe Institute studies in the sciences of complexity, Volume15), Addison Wesley Publishing Company (USA) 1994, pp 643.

46 Chau K.W., Wu, C.L. & Li, Y.S.,. Comparison of several flood forecasting models in Yangtze river, *J. Hydraul. Eng. - ASCE*, 10 (2005) 485-491.

47 Tripathi K. C., Das, I. M. L. & Sahai, A.K., Predictability of sea surface temperature in the Indian ocean region using artificial neural networks, *Indian. J. Mar. Sci.*, 35 (2006) 210–220.

48 Barman R., Kumar B. P., Pandey P. C. & Dubey S. K., Tsunami travel time prediction using neural networks, *Geophys. Res. Lett.*, 33(2006) doi:10.1029/2006GL026688.

49 Hsieh, W.W., Nonlinear canonical correlation analysis of the tropical pacific climate variability using a neural network approach, *J. Climate*, 14 (2001) 2528-2538.

50 Monahan A.H., Nonlinear principal component analysis by neural networks: theory and application to the Lorenz system, *J. Climate,* 13 (2000) 821-835.

51 Haas C., Liu Q. and Martin T., Retrieval of Antarctic sea ice pressure ridge frequencies from ERS SAR imagery by means of in-situ laser prolifing and usage of a neural network, *Int. J. Remote Sens*., 20 (1999) 3111-3123.

52 McIntire T. J. & Simpson J.J., Arctic sea ice, cloud, water, and lead classification using neural networks and 1.6μm data, *IEEE Trans. Geosci. Remote Sens.,* 40 (2002) 1956-1972.

53 Harms S., Fahrbach E. & Strass V. H., Sea ice transport in the Weddell Sea, *J. Geophys. Res.*, 106 (2001) 9057 – 9073.

54 Fichefet, T., Goosse, H. & Maqueda, M.A.M., A hindcast simulation of Arctic and Antarctic sea ice variability, 1955-2001, *Polar Res.*, 22 (2003) 91-98.

55 Comiso, J.C., Bootstrap sea ice concentrations from Nimbus-7 SMMR and DMSP SSM/ I, Boulder: National Snow and Ice Data Center, Digital media, 1999, updated 2002.

56 Wilks, D. S., *Statistical methods in the atmospheric sciences*, (Academic Press, USA) 1995, pp. 230-360.

57 Tsintikidis, D., Haferman, J.L., Anagnostou, E.N., Krajewski, W.F. & Smith, T.F., A neural network approach to estimating rainfall from spaceborne microwave data, *IEEE Trans. Geosci Remote Sens.*, 35 (1997) 1079-1093.

58 Cybenko G., Approximation by superposition of a sigmoidal function. *Math. Cont. Sig. Sys.*, 2 (1989) 303 - 314.

59 Hsieh, W.W. & Tang, B., Applying neural network models to prediction and data analysis in meteorology and oceanography, *Bull. Amer. Meteorol Soc.*, 79 (1998) 1855-1870.